Interfacial exchange-coupling induced chiral symmetry breaking of spin-orbit effects

P. Perna,[1,*] F. Ajejas,[1,2] D. Maccariello,[1,2] J. L. Fernandez Cuñado,[1,2] R. Guerrero,[1] M. A. Niño,[1]
A. Bollero,[1] R. Miranda,[1,2,3] and J. Camarero[1,2,3]

[1]*IMDEA-Nanoscience, c/ Faraday, 9 Campus de Cantoblanco, 28049 Madrid, Spain*
[2]*Departamento de Fisica de la Materia Condensada and Instituto "Nicolás Cabrera", Universidad Autónoma de Madrid,*
28049 Madrid, Spain
[3]*Condensed Matter Physics Center (IFIMAC), Universidad Autónoma de Madrid, 28049 Madrid, Spain*

We demonstrate that the interfacial exchange coupling in ferromagnetic/antiferromagnetic (FM/AFM) systems induces symmetry breaking of the spin-orbit (SO) effects. This has been done by studying the field and angle dependencies of anisotropic magnetoresistance and vectorial-resolved magnetization hysteresis loops, measured simultaneously and reproduced with numerical simulations. We show how the induced unidirectional magnetic anisotropy at the FM/AFM interface results in strong asymmetric transport behaviors, which are chiral around the magnetization hard-axis direction. Similar asymmetric features are anticipated in other SO-driven phenomena.

PACS number(s): 75.70.Tj, 75.30.Gw, 75.60.Jk, 85.75.−d

The spin-orbit (SO) interaction arises from the coupling of the electron spin with its orbital motion [1]. SO effects influence both magnetic and transport properties and constitute the subject of modern nanomagnetism. The microscopic origin of the magnetic anisotropy of ferromagnetic (FM) systems ultimately arises from SO [2], dictating the preferential magnetization directions. In FM/heavy metal structures, interfacial SO promotes a perpendicular magnetic anisotropy (PMA) [3] and it is responsible for chiral spin reversals [4], due to the Dzyaloshinskii-Moriya interaction (DMI) [5]. The SO interaction is exploited nowadays in spintronic applications [6], since it produces a mixing of the electron spin-up and spin-down states determining anisotropic magnetoresistive signals. In addition, SO-induced spin Hall effects may be exploited to efficiently manipulate and sense the magnetization in future spin-orbitronic applications [7]. In any case, transport phenomena are strongly influenced by the effective symmetry of the SO effects. Therefore, determining their general features represents a crucial step towards the understanding and the improvement of their functionalities.

In FM films with (twofold) uniaxial magnetic anisotropy (K_U), SO determines symmetric magnetoresistance (MR) responses around the magnetization easy-axis (e.a.) and hard-axis (h.a.) directions [8]: $\mathrm{MR}(\alpha,\mathbf{H}) = \mathrm{MR}(-\alpha,\mathbf{H}) = \mathrm{MR}(\alpha,-\mathbf{H})$, where α is the angle of the external applied magnetic field $\mathbf{H}$ with respect to the anisotropy direction. This is anisotropic magnetoresistance (AMR), which depends on the angle θ enclosed by the magnetization vector ($\mathbf{M}$) and the injected electrical current ($\mathbf{J}$) following a $\cos^2\theta$ law. Uniaxial systems present symmetric magnetization reversal pathways and hence symmetric MR responses. In this sense, a magnetic symmetry breaking could promote nonsymmetric reversals and MR responses. For instance, a FM layer exchange coupled with an antiferromagnet (AFM) layer presents an additional (onefold) unidirectional magnetic anisotropy (K_{EB}) [9], which is generally revealed through a shift of the hysteresis loop of the FM layer, called the exchange-bias (EB) field, and an enhancement of the coercivity. From a technological point of

view, EB is largely exploited in spintronics because it satisfies the need for stable and controlled MR outputs in magnetic recording, processing, and sensing devices. Systematic studies have shown how this interfacial exchange coupling modifies the magnetization reversal pathways [10,11]. The transport properties have also been studied, but only for several fixed magnetic field values and/or field directions [12–15].

In this Rapid Communication we show that the interfacial exchange coupling in FM/AFM systems strongly influences the SO effects, thus promoting asymmetric MR responses, which are chiral with respect to the h.a. direction, as Fig. 1 illustrates. Angular- and field-dependent measurements of the MR and the magnetization reversal pathways (measured simultaneously) have been reproduced with numerical simulations without any free parameter. We show how the symmetry of the MR response of an uniaxial FM system is broken by the unidirectional exchange coupling imposed by an adjacent AFM layer. In particular, symmetric MR responses are only found at characteristic magnetization directions (e.a. and h.a.).
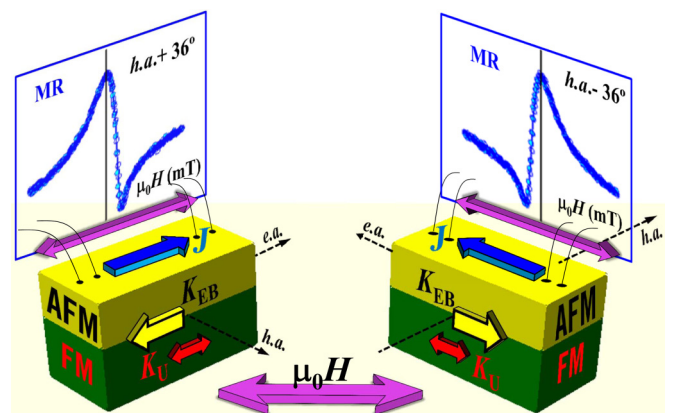

FIG. 1. (Color online) Schematic representation of the chiral asymmetric transport behavior in FM/AFM system (as described in the text), which arises from interfacial exchange coupling. The intrinsic (twofold) K_U and interfacial-induced (onefold) K_{EB} anisotropies are indicated with arrows. The top graphs display the corresponding MR curves acquired around the h.a. direction.

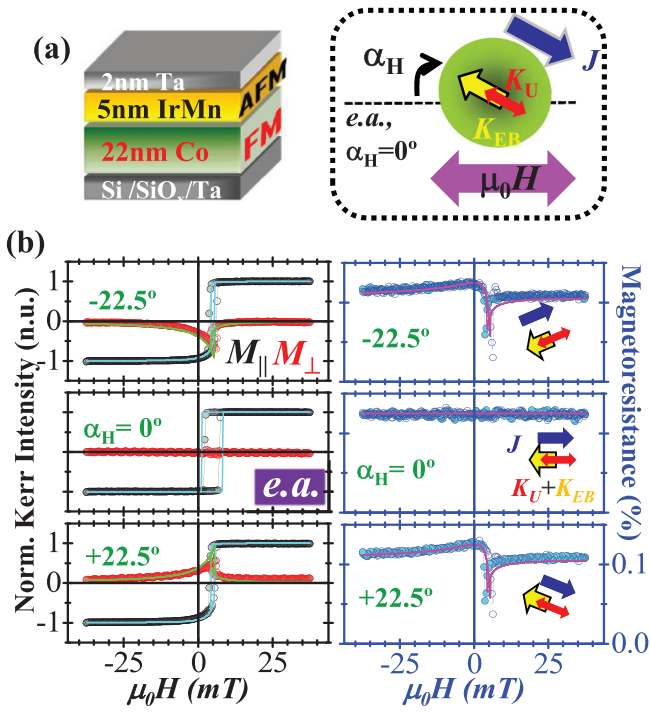─────────
*Corresponding author: paolo.perna@imdea.org

FIG. 2. (Color online) (a) Schemes of the sample structure (left) and experimental configuration (right), indicating the directions of the anisotropies (collinear K_U and K_{EB}), current ($\mathbf{J} \parallel K_U$), sample angle (α_H), and external magnetic field ($\mu_0 H$). (b) Magnetic and transport study at selected α_H around the e.a. direction. The left column panel shows the $M_\parallel/M_S$ and $M_\perp/M_S$ hysteresis field loops whereas the right column panel displays the corresponding MR loops. Symbols are the experimental data and the continuous lines are the corresponding simulated curves derived from the model described in the text. Solid (open) symbols refer to the descending (ascending) branch. The insets show schematically the specific current-anisotropy-field configuration. Notice the identical behavior of the MR(e.a. $\pm 22.5°$)-H curves.

Identical and chiral MR responses are observed around the e.a. and h.a. directions, respectively. Asymmetric magnetotransport behaviors produced by unidirectional symmetry breaking found in other spin-orbitronic systems are also discussed.

The scheme of the FM/AFM sample structure and the experimental configuration are shown in Fig. 2(a). Details on the fabrication of the FM/AFM bilayers and reference FM films, with collinear uniaxial K_U and unidirectional K_{EB}, are reported in the Supplemental Material [16]. Here, we refer to a 22 nm Co/5 nm IrMn bilayer because it presents the smallest anisotropy field [16].

The magnetic and transport properties were studied at room temperature (RT) by investigating the angular and field dependence of magnetization reversal pathways and magnetoresistive responses. Vectorial-resolved magnetization and resistance signals were acquired *simultaneously* as a function of the magnetic field for a given field orientation (α_H) [8]. $\alpha_H = 0°$ refers to when the anisotropy axis is oriented parallel to the external field [Fig. 2(a)]. The magnetization components, parallel ($M_\parallel$) and perpendicular ($M_\perp$) to the external field, were derived from vectorial-resolved magneto-optic

Kerr effect measurements [16–18]. The magnetoresistance (MR) was measured by using a lock-in amplifier in a four-probe method with the electrical current vector set parallel to the anisotropy axis (see Sec. II in Ref. [16]). The measurements were performed in the whole angular range. In general, the magnetization reverses via sharp irreversible (and smooth reversible) transitions, indicative of the nucleation and propagation of magnetic domains (magnetization rotation) [19]. The relevance of this refers to the proximity to the e.a. (h.a.) direction. Consequently, MR depends strongly on α_H.

The correlation between magnetic and transport properties and the general trends are determined from a comparison of the symmetry relationships between them. This will be discussed in details in the following, first by comparing field-dependent curves at selected angles around the characteristic e.a. [Fig. 2(b)] and h.a. (Figs. 3 and 4) directions, and then by comparing angle-dependent curves at selected fields (Fig. 5). It is worth remarking that the high symmetry found in the magnetotransport properties of a FM layer with uniaxial magnetic anisotropy is no longer satisfied in the FM/AFM system. At first glance, symmetric features in both magnetic and transport properties are found only at the easy and hard directions. In any other angular conditions, both magnetic and MR curves are strongly asymmetric.

Figure 2(b) compares representative vectorial-resolved magnetization (left panels) and magnetoresistance (right panels) hysteresis loops acquired simultaneously at selected α_H around the e.a. At $\alpha_H = 0°$ (central left panel), $M_\parallel$-H presents a shifted ($\mu_0 H_{EB} = +4.7$ mT) squared shape hysteresis loop with a sharp irreversible jump at 7.2 mT, whereas the $M_\perp$-H is negligible in the whole field loop. Away from the e.a., $M_\perp(H) \neq 0$ and reverses only in one semicircle, and above a critical angle, which depends on the ratio K_U/K_{EB} [10], the magnetization reversal becomes fully reversible. Therefore, close to the e.a. direction, nucleation and propagation of magnetic domains are the relevant processes. The right panels in Fig. 2(b) display the corresponding transport measurements. At the e.a., the MR-H curve is symmetric (and flat) in the whole field loop, whereas nonsymmetric curves are found for $\alpha_H \neq 0°$. As will be discussed below, similar features are found for $M_\parallel$-H and MR-H around the e.a. direction.

Figure 3 shows a similar study close to the h.a. In general, both $M_\parallel$ and $M_\perp$ loops show smooth reversible transitions, indicating that magnetization rotation is the relevant process during reversal. **M** rotates in plane only in one semicircle during the reversal, so that the angle between **M** and **J** is continuously changing as the field is sweeping. At the h.a. (central panels of Fig. 3), $M_\parallel$ displays a nearby linear behavior, with an anisotropy field $\mu_0 H_K = 9$ mT (see Sec. III of Ref. [16]), whereas MR shows the maximum variation, which yields 0.13%. In addition, the $M_\parallel$-H curve show rotational symmetry whereas $M_\perp$-H and MR-H curves are mirror symmetric with respect to zero field. However, these symmetric features are lost away from the h.a. direction.

Around the characteristic directions, different symmetry relationships are identified. For instance, for $\alpha_H = \pm 22.5°$, that is, around the e.a. direction [Fig. 2(b)], $M_\parallel$ and MR loops display identical field-dependent evolutions, i.e., $M_\parallel(\alpha_H, H) = M_\parallel(-\alpha_H, H)$ and MR$(\alpha_H, H) = $ MR$(-\alpha_H, H)$, whereas the $M_\perp$ experiences a sign change $M_\perp(\alpha_H, H) = $
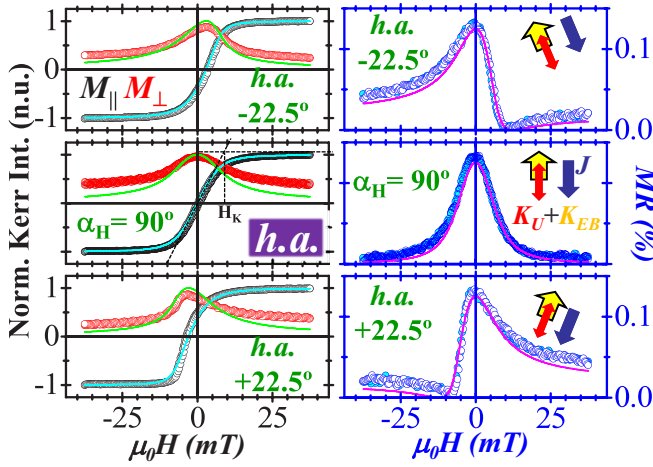
FIG. 3. (Color online) Magnetic and transport study at selected α_H around the h.a. with relevant magnetization rotation reversal. The left column panel shows the $M_\parallel/M_S$ and $M_\perp/M_S$ hysteresis field loops whereas the right column panel displays the corresponding MR loops. Symbols are the experimental data and the continuous lines are the corresponding simulated curves derived from the model described in the text. Solid (open) symbols refer to the descending (ascending) branch. The insets show schematically the specific current-anisotropy-field configuration. Note the chiral asymmetry behavior of the MR(h.a. $\pm$ 22.5°)-H curves.
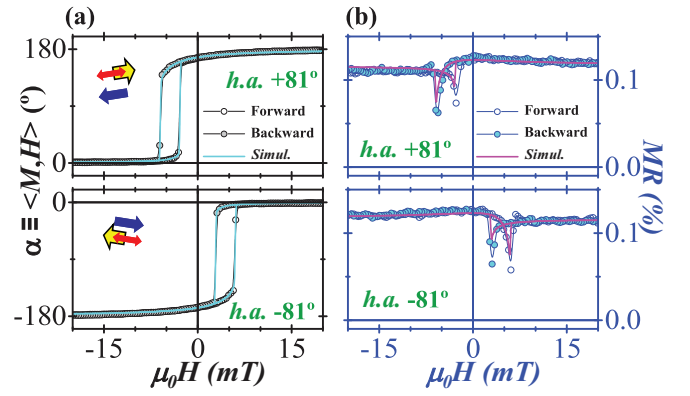

FIG. 4. (Color online) Magnetic and transport study at selected α_H around the h.a. with relevant domain nucleation and propagation reversal. The left column panel shows the hysteresis field loops of the angle of the magnetization vector [$\alpha \equiv \widehat{(\mathbf{M},\mathbf{H})}$] whereas the right column panel displays the corresponding MR loops. Symbols are the experimental data and the continuous lines are the corresponding simulated curves derived from the model described in the text. Solid (open) symbols refer to descending (ascending) branch. The insets show schematically the specific current-anisotropy-field configuration. Note the chiral asymmetry behavior of the MR(h.a.$\pm$81°)-H curves.

$-M_\perp(-\alpha_H, H)$. In turn, around the h.a. direction, e.g., for $\alpha_H = 90° \pm 22.5°$ (Fig. 3), the hysteresis curves of the parallel component are identical under rotation around the origin, i.e., $M_\parallel(\text{h.a.} + 22.5°, H) = -M_\parallel(\text{h.a.} - 22.5°, -H)$, whereas the hysteresis curves of the perpendicular component and the MR display chiral asymmetry, i.e., $M_\perp(\text{h.a.} + 22.5°, H) = M_\perp(\text{h.a.} - 22.5°, -H)$ and MR(h.a. $+ 22.5°, H) = $ MR(h.a. $- 22.5°, -H$). This [two-dimensional (2D)] chiral asymmetry is schematically illustrated in Fig. 1.

The chiral asymmetry is not only found close to the h.a., where the magnetization reversal is governed by magnetization rotation processes, but is extended in the whole angular range. Figure 4 shows the magnetic and transport behaviors for two selected field directions around the h.a., $\alpha_H = \text{h.a.} \pm 81°$, but very close to the e.a. direction, where reversal is governed by the nucleation and propagation of domains. In this case, Fig. 4(a) displays the hysteresis curves of the angle α of the magnetization vector with respect to the current direction extracted directly from the vectorial-Kerr data. This angle defines the magnetic torque. The corresponding resistance changes are shown in Fig. 4(b). In general, the MR loops present pronounced MR peaks, and in the meantime the magnetization switches from $\approx 0°$ to $\approx \pm 180°$. There is an asymmetry between the forward (descending) and backward (ascending) field branches in both magnetic and transport behaviors. This originates from the interfacial-induced unidirectional anisotropy which results with more rounded transitions and with higher MR peaks when the field sweeps against the unidirectional anisotropy [10,13]. Moreover, the chiral asymmetry is preserved, i.e., MR(h.a. $+ 81°, H) = $ MR(h.a.$-81°, -H$). This indicates that this asymmetry is independent of the reversal mechanism.

To gain further insight into the symmetry breaking of the SO effects, we have performed numerical simulations by using a modified coherent rotation Stoner-Wohlfarth (SW) model (with no free parameters) in which we included collinear uniaxial and unidirectional anisotropy terms with $K_U/K_{EB} = 0.37$ (see Secs. III and IV of Ref. [16]). This allows us to simulate the angular and magnetic field dependence of the magnetization reversal pathways [11], i.e., $M_\parallel(\alpha_H, H), M_\perp(\alpha_H, H)$, and to derive the corresponding MR responses according to MR$(\alpha_H, H) \propto \cos^2\theta(\alpha_H, H)$, where $\theta \equiv \widehat{(\mathbf{M},\mathbf{J})}$. The simulated hysteresis curves are superimposed [continuous black lines in Figs. 2(b), 3, and 4] to the experimental curves. There is a perfect agreement between them, including their asymmetries, which demonstrates that both magnetization pathways and magnetoresistance responses are strongly affected by the system symmetry.

The broken symmetry of the SO effects can be clearly observed by plotting the whole angular evolution of the MR-H hysteresis loops in a 2D map representation [Fig. 5(a)]. Such a plot allows one to visualize the broken periodicity. While the well-defined uniaxial (twofold) magnetic anisotropy of a FM results with a 180° periodicity [8], the additional unidirectional (onefold) anisotropy induced at the FM/AFM interface promotes the symmetry breaking of the SO effects [16], resulting in a 360° periodicity.

In order to visualize the angle dependence of MR, different horizontal cuts of the 2D map have been plotted in the top graph in Fig. 5(a). This represents the angular evolution of MR at different magnetic field values. At remanence (i.e., $\mu_0 H = 0$ mT, blue open circles), the MR signal comes out from a $\mathbf{M}\parallel\mathbf{J}$ configuration in the whole angular range and therefore it does not change. For a nonzero external field, the angular dependence of the MR is clearly asymmetric, as the mirror
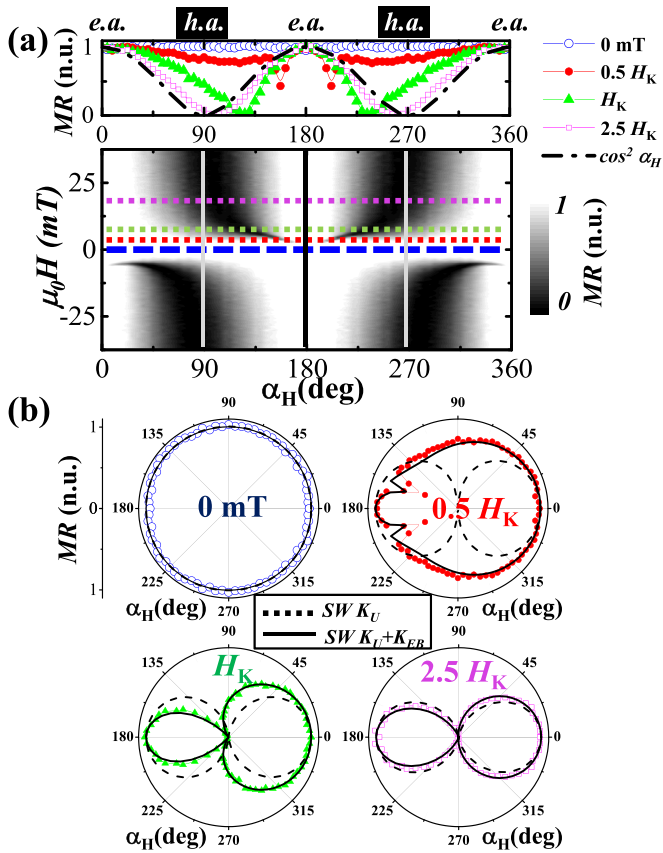
FIG. 5. (Color online) (a) Bottom graph: 2D field-angular map representation of the magnetoresistance MR derived from the forward field-branch hysteresis curves acquired at different angles, as the ones shown in the right panels of Figs. 2–4 (similar information can be derived from the backward 2D map [16]). The h.a. (e.a.) directions are indicated with vertical gray (black) continuous lines. The dashed lines indicate the corresponding horizontal cuts at selected fields displayed in the top graph. Notice that the MR angular dependence is approaching a $\cos^2 \alpha_H$ law (represented with a dotted-dashed curve) for fields much larger than the anisotropy field H_K. (b) Polar-plot representation of the angular dependence of the MR for different fields. Symbols are the experimental data. Solid (dashed) curves are derived from numerical simulation for the FM/AFM bilayer (single FM reference film). Note that both come closer at high fields whereas at low fields they are very different. Remarkably, for the (unidirectional) exchange-biased system, the chiral asymmetry around the h.a. direction is reproduced.

symmetry along the horizontal axis is completely broken. From a simple inspection of the top graph of Fig. 5(a), we can figure out relevant information. First, the maximum values of the MR are found when α_H is aligned along the anisotropy direction. **M** is parallel to **J** only in a small range of angles, which increases as the external field increases. Away from the anisotropy direction, the MR value decreases gradually and it is minimum where the angle between **M** and **J** approaches 90°. Second, larger MR changes are found as the external field increases. Third, the MR displays identical or different (asymmetry) values around the anisotropy or h.a. direction, respectively. The asymmetry vanishes for very large external magnetic fields compared to the anisotropy field, where the angle dependence of MR approaches a $\cos^2 \alpha_H$ law.

The discussed trends and symmetry-breaking SO effects are also reflected in the corresponding polar-plot representation of the MR shown in Fig. 5(b). Each graph includes both experimental (symbols) and simulated (lines) data. The latter include model uniaxial (SW K_u) and exchange-biased (SW $K_u + K_{EB}$) systems. In remanence conditions, both models are indistinguishable, i.e., a circular-shaped polar plot with no MR variation. For $\mu_0 H \neq 0$, the simulated polar plots of the uniaxial system display a similar two-lobe behavior, which result with mirror symmetry with respect to both the e.a. and h.a. directions. In contrast, the simulated polar plots of the exchange-biased system show mirror symmetry with respect to the e.a. direction and a (chiral) asymmetry with respect to the h.a. direction. The asymmetry diminishes as the external field increases, vanishing for very large fields compared with the anisotropy field. Remarkably, all experimental data are very well reproduced by the model (see also Sec. IV of Ref. [16]).

Asymmetric transport and magnetic behaviors, originating from interfacial symmetry-breaking (unidirectional) effects, can also be found in other magnetic systems. For instance, exchange-biased spin valves display chiral symmetry in both magnetization and giant magnetoresistance loops around the h.a. direction (see the graph panels of Fig. 2 in Ref. [20]), as well as asymmetric MR curves were found in exchange-biased multiferroic BiFeO$_3$-based systems [21]. In addition, fixed chiral spin structures can be stabilized in PMA systems with sizable DMIs [22], and in the presence of an in-plane magnetic field, producing asymmetric magnetization reversal features during (chiral) magnetic domain nucleation [23] and domain propagation [24]. On the other hand, in FM/HM systems with in-plane magnetization, a SO-dependent effective in-plane field has been demonstrated, giving rise to asymmetric reversal [25]. Asymmetric planar Hall [26] and inverse spin Hall [27] effect signals have also been recently reported in exchange-biased insulating FM/metallic AFM bilayers, as well as asymmetries in the spin Hall magnetoresistance have been found in SrMnO$_3$/Pt [28]. These asymmetric signals, which are generally clearly observed at low magnetic fields, arise from the SO coupling in the presence of an unidirectional magnetic anisotropy. In the large field regime, the asymmetries vanish, in agreement with our results.

In summary, we have demonstrated the existence of broken symmetry of the SO effects due to the exchange interaction at the FM/AFM interface, which is responsible for asymmetries in both magnetic and transport properties. In particular, we have shown an intrinsic chiral asymmetry in the MR with respect to the magnetization hard-axis direction. Similar effects can be envisaged for other spintronic and spin-orbitronic systems when either intrinsic magnetic anisotropy or the SO interaction presents symmetry breaking.

[1] T. R. McGuire and R. I. Potter, IEEE Trans. Magn. **11**, 1018 (1975).

[2] *Metallic Multilayers and their Applications*, edited by G. W. Fernando, Handbook of Metal Physics, Vol. 4 (Elsevier, Amsterdam, 2008).

[3] J. Stöhr, J. Magn. Magn. Mater. **200**, 470 (1999).

[4] A. N. Bogdanov and U. K. Rößler, Phys. Rev. Lett. **87**, 037203 (2001).

[5] A. Fert, Mater. Sci. Forum **59-60**, 439 (1990); A. Fert and P. M. Levy, Phys. Rev. Lett. **44**, 1538 (1980); A. Fert, V. Cros, and J. Sampaio, Nat. Nanotechnol. **8**, 152 (2013).

[6] C. Chappert, A. Fert and F. Nguyen Van Dau, Nat. Mater. **6**, 813 (2007).

[7] A. Hoffmann, IEEE Trans. Magn. **49**, 5172 (2013).

[8] P. Perna, D. Maccariello, C. Rodrigo, J. L. F. Cuñado, M. Muñoz, J. L. Prieto, M. A. Niño, A. Bollero, J. Camarero, and R. Miranda, Appl. Phys. Lett. **104**, 202407 (2014).

[9] J. Nogues and I. K. Schuller, J. Magn. Magn. Mater. **192**, 203 (1999).

[10] J. Camarero, J. Sort, A. Hoffmann, J. M. Garcia-Martin, B. Dieny, R. Miranda, and J. Nogues, Phys. Rev. Lett. **95**, 057204 (2005).

[11] E. Jiménez, J. Camarero, J. Sort, J. Nogues, N. Mikuszeit, J. M. Garcia-Martin, A. Hoffmann, B. Dieny, and R. Miranda, Phys. Rev. B **80**, 014415 (2009).

[12] B. H. Miller and E. D. Dahlberg, Appl. Phys. Lett. **69**, 3932 (1996).

[13] S. Brems, K. Temst, and C. Van Haesendonck, Phys. Rev. Lett. **99**, 067201 (2007).

[14] M. Gruyters, J. Appl. Phys. **95**, 2587 (2004).

[15] K.-U. Barholz and R. Mattheis, IEEE Trans. Magn. **38**, 2767 (2002).

[16] See Supplemental Material at http://link.aps.org/supplemental/10.1103/PhysRevB.92.220422 for detailed information on experimental/simulation procedures and extended data.

[17] E. Jiménez, N. Mikuszeit, J. L. F. Cuñado, P. Perna, J. Pedrosa, D. Maccariello, C. Rodrigo, M. A. Niño, A. Bollero, J. Camarero, and R. Miranda, Rev. Sci. Instrum. **85**, 053904 (2014);

J. L. F. Cuñado, J. Pedrosa, F. Ajejas, A. Bollero, P. Perna, F. J. Teran, R. Miranda, and J. Camarero, *ibid.* **86**, 046109 (2015).

[18] P. Perna, C. Rodrigo, E. Jiménez, F. J. Teran, N. Mikuszeit, L. Méchin, J. Camarero, and R. Miranda, J. Appl. Phys. **110**, 013919 (2011); P. Perna, C. Rodrigo, E. Jiménez, N. Mikuszeit, F. J. Teran, L. Méchin, J. Camarero, and R. Miranda, *ibid.* **109**, 07B107 (2011).

[19] P. Perna, L. Méchin, M. Saïb, J. Camarero, and S. Flament, New J. Phys. **12**, 103033 (2010).

[20] P. Perna, C. Rodrigo, M. Muñoz, J. L. Prieto, A. Bollero, D. Maccariello, J. L. F. Cuñado, M. Romera, J. Akerman, E. Jiménez, N. Mikuszeit, V. Cros, J. Camarero, and R. Miranda, Phys. Rev. B **86**, 024421 (2012).

[21] J. Allibe, S. Fusil, K. Bouzehouane, C. Daumont, D. Sando, E. Jacquet, C. Deranlot, M. Bibes, and A. Barthelemy, Nano Lett. **12**, 1141 (2012).

[22] G. Chen, J. Zhu, A. Quesada, J. Li, A. T. N'Diaye, Y. Huo, T. P. Ma, Y. Chen, H. Y. Kwon, C. Won, Z. Q. Qiu, A. K. Schmid, and Y. Z. Wu, Phys. Rev. Lett. **110**, 177204 (2013).

[23] S. Pizzini, J. Vogel, S. Rohart, L. D. Buda-Prejbeanu, E. Jué, O. Boulle, I. M. Miron, C. K. Safeer, S. Auffret, G. Gaudin, and A. Thiaville, Phys. Rev. Lett. **113**, 047203 (2014).

[24] A. Hrabec, N. A. Porter, A. Wells, M. J. Benitez, G. Burnell, S. McVitie, D. McGrouther, T. A. Moore, and C. H. Marrows, Phys. Rev. B **90**, 020402(R) (2014).

[25] X. Fan, J. Wu, Y. Chen, M. J. Jerry, H. Zhang, and J. Q. Xiao, Nat. Commun. **4**, 1799 (2013).

[26] X. Zhou, L. Ma, Z. Shi, W. J. Fan, R. F. L. Evans, J.-G. Zheng, R. W. Chantrell, S. Mangin, H. W. Zhang, and S. M. Zhou, Sci. Rep. **5**, 9183 (2015).

[27] C. Du, H. Wang, F. Yang, and P. C. Hammel, Phys. Rev. B **90**, 140407(R) (2014).

[28] J. H. Han, C. Song, F. Li, Y. Y. Wang, G. Y. Wang, Q. H. Yang, and F. Pan, Phys. Rev. B **90**, 144431 (2014).